Nonlinear inversion for ocean-bottom properties

Michael D. Collins and W. A. Kuperman
Naval Research Laboratory, Washington, DC 20375

Henrik Schmidt
Massachusetts Institute of Technology, Cambridge, Massachusetts 02139

(Received 6 March 1992; accepted for publication 8 July 1992)

High-resolution methods based on simulated annealing and full-wave sound propagation models are developed for nonlinear inversion for ocean-bottom properties. Simulated annealing is used to search the high-dimensional parameter space of ocean bottoms for the parameter set corresponding to the best replica field. The parabolic equation method is used to solve range-dependent inversion problems. For data taken by Lynch *et al.* from a range-dependent region of the Gulf of Mexico [J. Acoust. Soc. Am. **89**, 648–665 (1991)], this approach achieves excellent agreement between the theoretical and measured acoustic pressures. The recovered sediment parameters suggest that a sound-speed boundary layer exists in the upper part of the sediment and that the depth of an interface in the sediment is range dependent. For locally range-independent problems, inversion is performed in wave-number space. Large efficiency gains are possible with this approach because the number of wave-number samples required for inversion is much smaller than the number of wave-number samples required for computing replica fields.

PACS numbers: 43.30.Bp, 43.30.Ft, 43.30.Ma, 43.30.Pc

INTRODUCTION

In principle, data obtained using acoustic sources and receivers located in the water column as illustrated in Fig. 1 may be sufficient for determining the properties of the ocean bottom. In practice, it is difficult to extract this information because the wave equation must be solved repeatedly while searching a parameter space that describes the ocean bottom for the optimal parameter values. In the past, this inverse problem has been simplified by using idealized propagation models, linear optimization methods, perturbation methods, and other approaches.[1–5] In this paper, we develop methods for inverting for the properties of the ocean bottom based on nonlinear optimization and sound propagation models designed to solve realistic problems. These methods are tested using real and simulated data.

The ocean bottom is parametrized and an energy function that depends on the array data and the replica field is minimized. This matched-field approach has been used to solve other ocean acoustics inverse problems, including source localization and tomography.[6–9] The replica field corresponds to theoretical array data and is constructed for each test ocean bottom by solving the wave equation. In general, a nonlinear optimization method is required to search the parameter space because the energy function may have local minima. We solve the inversion problem using simulated annealing, an efficient nonlinear optimization method for problems involving large numbers of parameters[10,11] that has been applied to various inverse problems.[12,13] The simulated annealing algorithm that we use for inverting ocean-bottom properties is described in Appendix A.

In Sec. II, we develop a nonlinear inversion method based on the parabolic equation (PE) method[14] and test the method using simulated data. The PE method is an efficient range-dependent propagation model that handles elastic sediments[15] and the wide-angle propagation paths that penetrate deeply into the ocean bottom and return to the water column in the nearfield.[16] In Sec. III, the PE-based inversion method is applied to a set of data taken by Lynch *et al.* from a gradually range-dependent region of the Gulf of Mexico. Their inversion with a linear optimization method and a range-independent propagation model achieved fairly good agreement between the theoretical and measured acoustic fields.[3] The PE-based inversion method achieves excellent agreement between the theoretical and measured acoustic

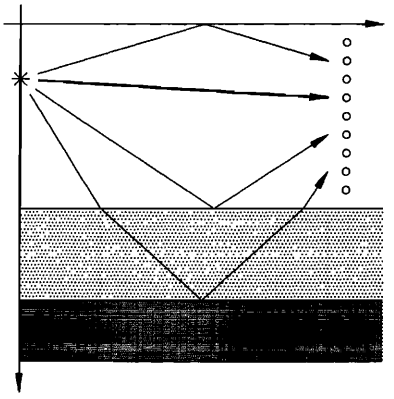

FIG. 1. A sample configuration of the source and receivers for a problem involving two sediment layers. The bottom-interacting propagation paths contain information about the sediment properties. The direct arrival and the surface-reflected arrival are regarded as noise for the inversion problem.

 0001-4966/92/112770-14$00.80

fields. The results suggest that a sound-speed boundary layer (in which sound speed varies rapidly with depth) exists in the upper part of the sediment and that the depth of the interface between the upper two sediment layers is range dependent.

In Sec. IV, we develop a nonlinear inversion method based on matching the wave-number spectrum, which is applicable to locally range-independent problems. This approach is very efficient for some range-independent problems. Other inversion methods based on matching the wave-number spectrum have been developed previously.[17,18] Performing inversion in wave-number space can significantly reduce computation times because many more wave-number samples are required to construct solutions of the wave equation than to perform inversion. We construct replica fields with an efficient spectral model for solving the elastic wave equation.[19,20] An important step in wave-number inversion is the estimation of the wave-number spectrum, including the extrapolation of the field to long ranges so that the acoustic pressure may be transformed numerically.

I. GENERAL ASPECTS OF INVERSION

In this section, we discuss general aspects of inversion for ocean-bottom properties. A sound source (or possibly an array of sound sources) and an array of receivers are placed in the water column at known locations. A finite-dimensional parameter space is defined to describe a set of test ocean bottoms. An energy function is defined to quantify the agreement of the data (the acoustic fields measured at the receivers) with the replica fields (solutions of the wave equation). An optimization method is used to minimize the energy function over the parameter space. The performance of the inversion depends on the experimental configuration and the computational techniques.

A. Experimental configuration

The frequency content of the source array is an important performance factor. Since sediment attenuation increases with frequency, low-frequency signals can probe deeper into the ocean bottom. High-frequency sources can resolve finer details in the upper part of the ocean bottom. The most simple source array consists of a single cw source. This is the least effective source array because the relatively weak bottom-interacting arrivals are superimposed both spatially and temporally on the water-borne arrivals. The performance of inversion can be improved by using an array of cw sources phased so that the ocean bottom is ensonified by a beam and the water-borne arrivals are nearly eliminated or by using a broadband source so that bottom-interacting energy arrives separately. Since it is relatively difficult to deploy arrays of phased sources and to solve broadband propagation problems, it might be necessary in practice to work with a single source and a small number of discrete frequencies.

The location and geometry of the receiver array are important performance factors. Performance may be improved by choosing the receiver locations to maximize the signal-to-noise ratio (i.e., minimize the ratio of the total received energy to energy received from bottom-interacting propagation paths). This may be a practical alternative to using a beamed source array or a broadband source. The direct and surface-reflected arrivals, which contain no information about the ocean bottom, can be reduced by placing the receivers in the null directions of the Lloyd's mirror beams. When the upper part of the water column is downward refracting, the shadow zone is an effective location for the receivers. To determine properties deeply within the ocean bottom, it is best to place the receivers at relatively short ranges because the magnitude of bottom-interacting energy decreases rapidly with range. A vertical array of receivers is the logical choice for this purpose. For near-field receivers, the signal-to-noise ratio is higher, less computation time is required for some propagation models, and the receiver ranges are easier to measure.

Horizontal arrays also have advantages for the inversion problem. Horizontal arrays are more effective than vertical arrays for range-dependent inversion problems. For example, the solution may not be unique for vertical array data if mode coupling[21] does not occur.[8] In contrast to vertical arrays, the length of a horizontal array is not limited by the depth of the ocean. The properties of the upper sediment layers, which have the greatest effect on long-range propagation, may be estimated accurately with a horizontal array that covers several kilometers. Inversion with a horizontal array requires less hardware than inversion with a vertical array. For example, the synthetic aperture approach used to collect the data of Ref. 3 requires only one receiver.

B. Computational techniques

There are several sound propagation models for computing replica fields. For the inversion problem, it is important to select a model that handles realistic problems accurately. Although near-field accuracy is desirable for the inversion problem, achieving far-field accuracy has tended to be the major goal of underwater sound propagation modeling. Efficiency is an important factor because the wave equation must be solved many times during the parameter search. To handle even the simplest inversion problems, it is necessary to solve the acoustic wave equation for depth-dependent ocean environments. Since many ocean bottoms have layers that support shear waves, it is often necessary to solve the elastic wave equation. In some ocean environments, the region spanned by the source and receiver arrays must be regarded as both depth and range dependent.

It is important to parametrize efficiently because the likelihood of ambiguous solutions increases with the number of unknown parameters. It is also important that the parametrization is realistic because there is no chance of success if none of the ocean bottoms in the parameter space resembles the true ocean bottom. *A priori* information is very useful for achieving an efficient and realistic parametrization. The unknowns in the ocean bottom may include the compressional speed, shear speed, density, compressional attenuation, shear attenuation, locations of interfaces be-

tween layers of different material types, and other quantities. The unknowns may also include quantities such as the sound speed in the water column and corrections to the positions of the sources and receivers.

If the available *a priori* information is limited, inversion may require a nonlinear optimization method for searching the parameter landscape for the global minimum of the energy function. It is important to tune the search algorithm to the inversion problem to reduce the number of replica fields that must be computed.

II. INVERSION WITH THE PE METHOD

In this section, we develop a PE-based inversion method and perform tests using simulated data. This inversion method may be applied to problems involving range and depth dependence. We work in cylindrical coordinates with r being the range from the source and z being the depth below the ocean surface. For arrays with horizontal aperture, the cylindrical spreading factor $r^{-1/2}$ is removed from the complex pressure P. The basic ocean-bottom acoustic parameters are the sound speed c, the density ρ, and the attenuation β. For the water column, we assume that c is known and that $\rho = 1$ g/cm^3 and $\beta = 0$. The jth search parameter is denoted by X_j, which is required to remain within the interval (A_j, B_j), with the true value Y_j. The value of X_j corresponding to the lowest energy state encountered in the simulated annealing search is denoted by $\tilde{X}_j$.

In the past, most PE models designed for ocean acoustics used a pressure-release boundary condition at the bottom boundary that truncates the computational grid. To avoid artificial reflections, this boundary is placed deep in the sediment, and the attenuation is assigned artificially large values in its vicinity. This approach is least effective at short ranges, where the acoustic field is rich with information about the sediment parameters. To improve the efficiency of our PE model for inversion, we have implemented the radiation boundary conditions (RBCs) that are described in Appendix B and are related to the RBCs of Ref. 22.

The data vector $\mathbf{P}$ contains the complex pressures P_n measured at the receivers in an N-element array. The normalized data vector $\hat{\mathbf{P}}$ is defined by

$$\hat{\mathbf{P}} = |\mathbf{P}|^{-1}\mathbf{P} = (\hat{P}_1, \hat{P}_2, \ldots, \hat{P}_N), \tag{1}$$

$$|\mathbf{P}| = \sqrt{\sum_{n=1}^{N} |P_n|^2}. \tag{2}$$

The replica vector $\mathbf{Q}$ contains the complex pressures Q_n computed using the test parameters.

When it is possible to measure phases accurately, we use the following energy function:

$$E = \min_{\lambda} |\mathbf{P}|^{-1} |\mathbf{P} - \lambda \mathbf{Q}|. \tag{3}$$

We show in Appendix C that this energy function, which does not require knowledge of the source phase or amplitude, reduces to

$$E = \sqrt{1 - |\hat{\mathbf{P}}^* \hat{\mathbf{Q}}|^2}, \tag{4}$$

TABLE I. The parameters for example A, which involves a range-dependent environment and inversion with the PE method. The values for $\tilde{X}_j$ appear in separate columns for a single source and for an array of sources.

j	Y_j	A_j	B_j	Single	Array	Units
1	1550	1500	1600	1517.4	1541.7	m/s
2	1600	1550	1650	1609.5	1600.5	m/s
3	1700	1600	1850	1677.1	1702.1	m/s
4	1750	1650	1900	1782.1	1750.9	m/s
5	1850	1700	2100	1864.4	1851.1	m/s
6	1.2	1.1	1.4	1.22	1.19	g/cm^3
7	0.2	0.1	0.4	0.341	0.199	dB/λ

where the superscript asterisk denotes complex conjugation. Since it may take hours to collect data over a long synthetic aperture array, it may not be practical to measure phases accurately in some cases. For this situation, we use the following energy function:

$$E = \sqrt{\sum_{n=1}^{N} (|\hat{P}_n| - |\hat{Q}_n|)^2}. \tag{5}$$

Example A is a range-dependent problem for which the ocean depth decreases linearly from 400 to 350 m over the first 2 km in range from a 25-Hz source array. We take $c = 1500$ m/s in the water column. In the sediment, ρ and β are constant and $c(z)$ is continuous, linear between the nodes $z = z_j = (300 + 50j)$ m for $j \leqslant 5$, and constant for $z > z_5$. In the sediment, the search parameters are $X_j = c(z_j)$ for $j \leqslant 5$, $X_6 = \rho$, and $X_7 = \beta$. We consider the case of a single source at $z = 200$ m and the case of an array of ten sources beamed 45 deg below the horizontal, with the jth source at $z = (30j)$ m. Table I contains parameters and results for example A.

The dependence of the acoustic field on the range of the receivers and the type of source is illustrated in Fig. 2. At both $r = 1$ km and $r = 2$ km, $P(z)$ is more sensitive in the water column to perturbations of X_5 for the source array than for the single source. Since the sensitivity is greatest at $r = 2$ km, we perform inversion using a vertical array of 20 receivers at this range, with the jth receiver at $z = (15j)$ m. We use the energy function given by Eq. (4). The dependence of E on each of the parameters is illustrated in Fig. 3 for both of the sources. The jth curve in Fig. 3 corresponds to E as X_j varies over (A_j, B_j) while $X_i = Y_i$ for $i \neq j$. We observe that E is relatively insensitive to variations in X_1, X_2, X_6, and X_7. Sensitivity to density and attenuation perturbations tends to be low for most problems. For this problem, sensitivity is also low for X_1 and X_2 because only a fraction of the upper segment of the sound-speed profile is sampled at each range. Sensitivity to variations in X_5 is relatively low for the single source and high for the array of sources. Both of the curves for X_5 have local minima.

We applied the simulated annealing algorithm described in Appendix A to this problem using $T_0 = 5$. The results of 250 iterations appear in Fig. 4 for a single source and Fig. 5 for an array of sources. The annealing was quenched (i.e., T was set to zero) after 230 iterations. Each

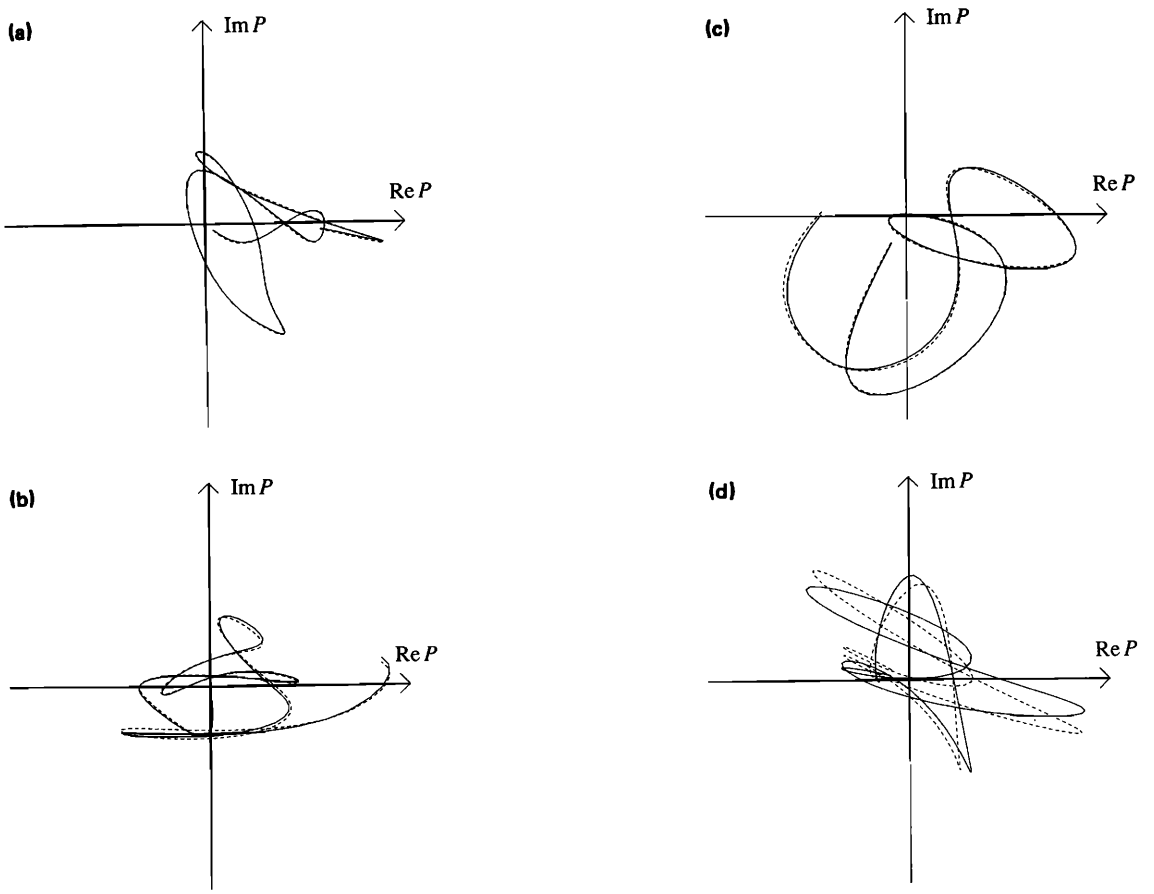

FIG. 2. Mappings of the complex pressure $P(z)$ for example A, which involves a range-dependent environment, onto the complex plane as z sweeps over the water column. The solid curves correspond to the true parameters. The dashed curves correspond to perturbing X_5, the sound speed at the node at $z = 550$ m, by 5 m/s. (a) A single source at $r = 1$ km. (b) An array of sources at $r = 1$ km. (c) A single source at $r = 2$ km. (d) An array of sources at $r = 2$ km.

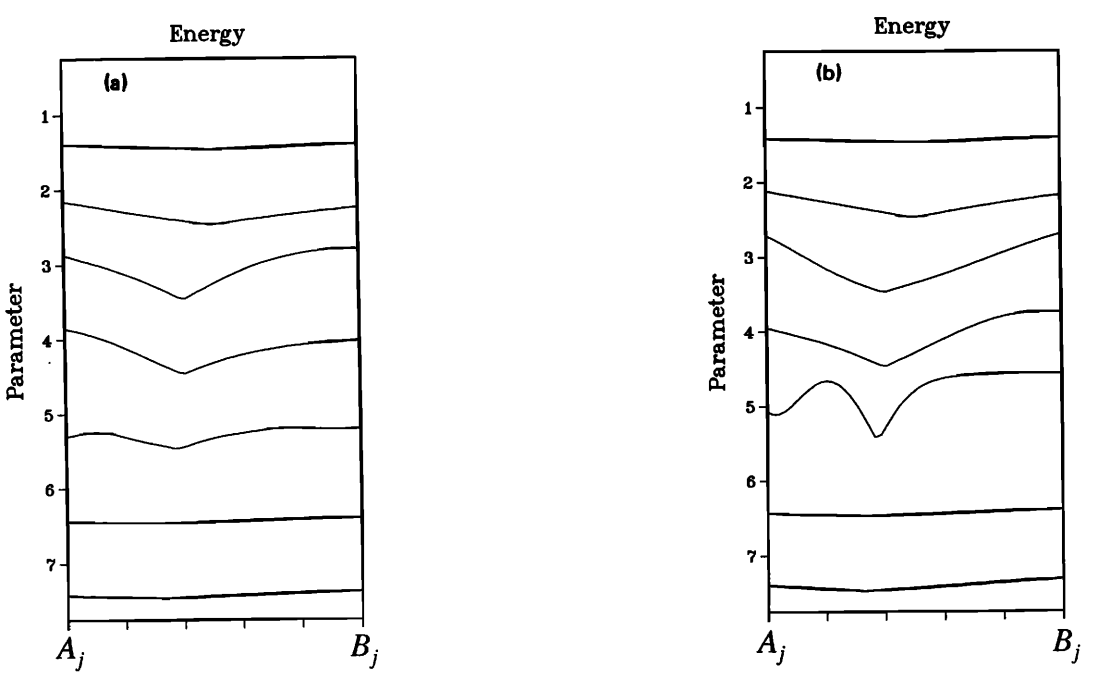

FIG. 3. The dependence of the energy function for example A, which involves a range-dependent environment, on the parameters for (a) a single source and (b) an array of sources. Along the horizontal axis, X_j varies from A_j to B_j while $X_i = Y_i$ for $i \neq j$.

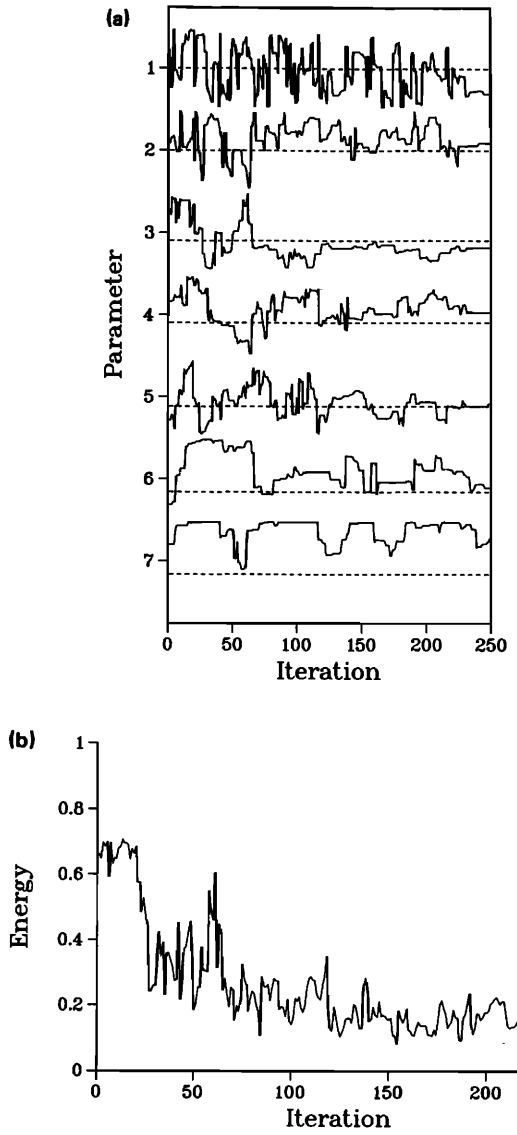

FIG. 4. Results for example A, which involves a range-dependent environment. Inversion using a single source. (a) Convergence of the parameters to the true values (dashed lines). (b) The energy function.

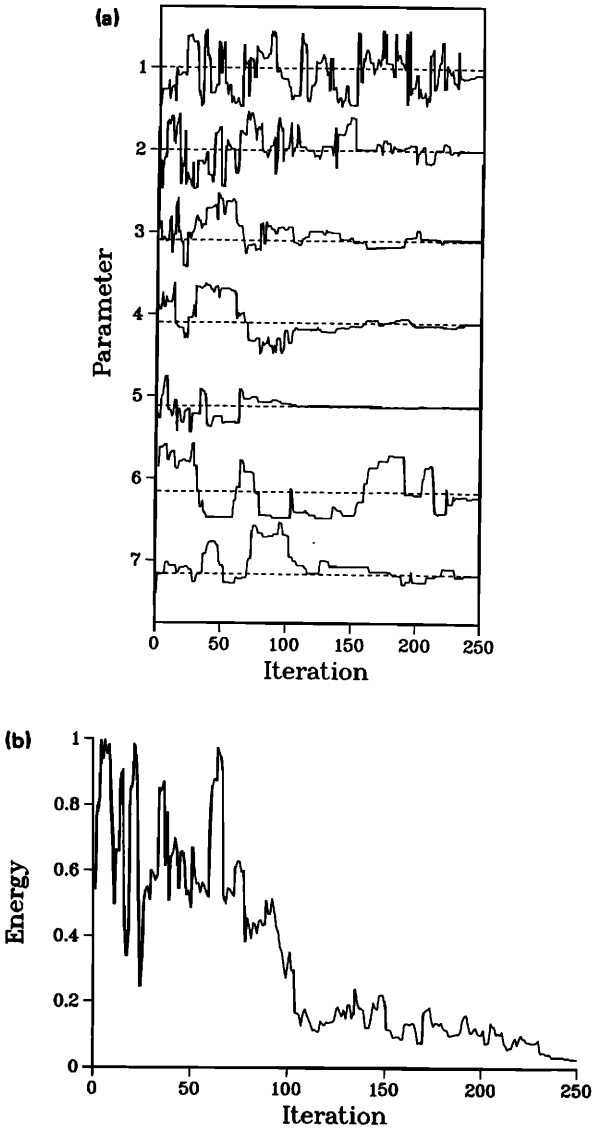

FIG. 5. Results for example A, which involves a range-dependent environment. Inversion using an array of sources. (a) Convergence of the parameters to the true values (dashed lines). (b) The energy function.

of these simulations involved 1750 PE runs and required about 7 min of run time on a Cray X-MP/24 computer. For the inversion with a single source, all of the parameters are recovered fairly well except for β. For the inversion with an array of sources, all of the parameters are recovered, and some of them are strongly attracted to the true values.

Example B is a range-independent problem involving a 50-Hz source at $z = 25$ m in an ocean of depth 100 m. We take $c = 1500$ m/s in the water column. The ocean bottom consists of a 100-m-thick upper layer overlying a homogeneous basement layer. The parameters X_1 and X_2 are the values of the linear sound speed in the upper layer at $z = 100$ m and $z = 200$ m. The parameters X_3 and X_4 correspond to the constant ρ and β in the upper layer. The parameters X_5, X_6, and X_7 correspond to c, ρ, and β in the basement layer. Table II contains parameters and results for example *B*. For $r \geqslant 400$ m, the receivers are placed at $z = 95$ m and are separated by 20 m in range.

We applied the simulated annealing algorithm to this problem using the energy function defined by Eq. (5) and $T_0 = 10$. The results of 500 iterations appear in Figs. 6, 7, and 8 for arrays stretching out to 1, 2, and 4 km. The anneal-

TABLE II. The parameters for example B, which involves a two-layer sediment and inversion with the PE method. The values for $\tilde{X}_j$ appear in separate columns for the maximum ranges of 1, 2, and 4 km.

j	Y_j	A_j	B_j	1 km	2 km	4 km	Units
1	1530	1500	1650	1532.4	1530.1	1529.5	m/s
2	1600	1550	1700	1598.8	1599.4	1599.0	m/s
3	1.2	1.1	1.4	1.21	1.24	1.23	g/cm^3
4	0.05	0.0	0.1	0.031	0.051	0.054	dB/λ
5	1750	1600	1800	1748.7	1752.8	1750.8	m/s
6	1.4	1.15	1.5	1.41	1.43	1.35	g/cm^3
7	0.35	0.1	0.5	0.357	0.359	0.258	dB/λ

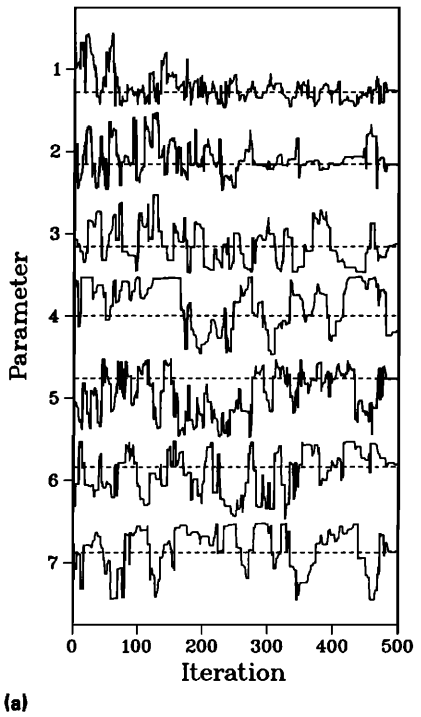

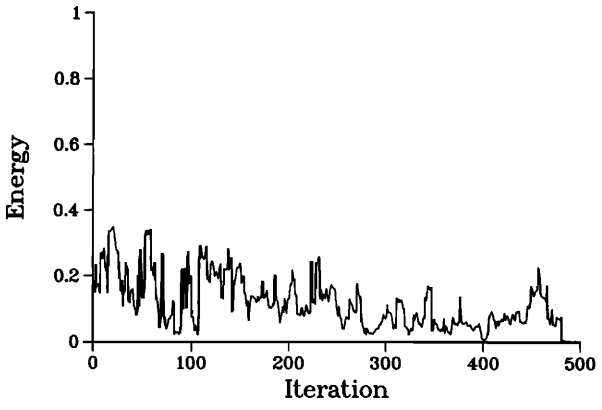

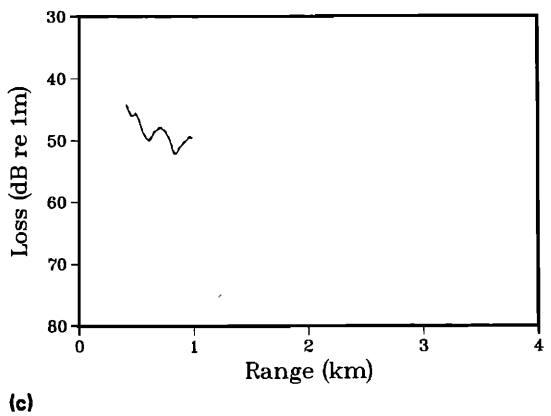

FIG. 6. Results for example B, which involves a range-independent ocean overlying a two-layer sediment. Inversion using a horizontal array that stretches out to $r = 1$ km. (a) Convergence of the parameters to the true values (dashed lines). (b) The energy function. (c) Transmission loss curves for the parameters corresponding to the lowest energy state encountered (solid curve) and for the true parameters (dashed curve).

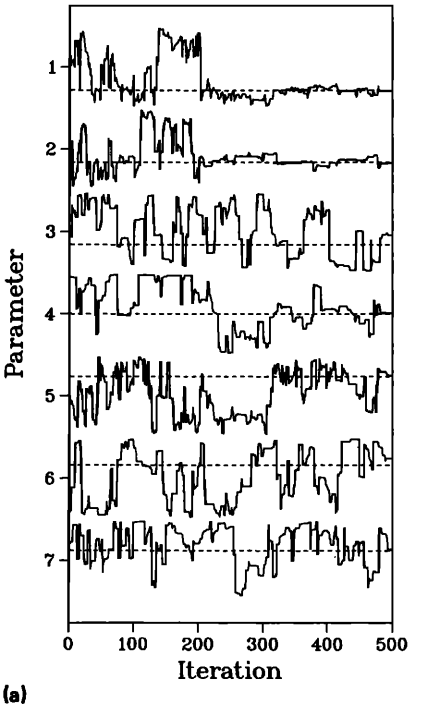

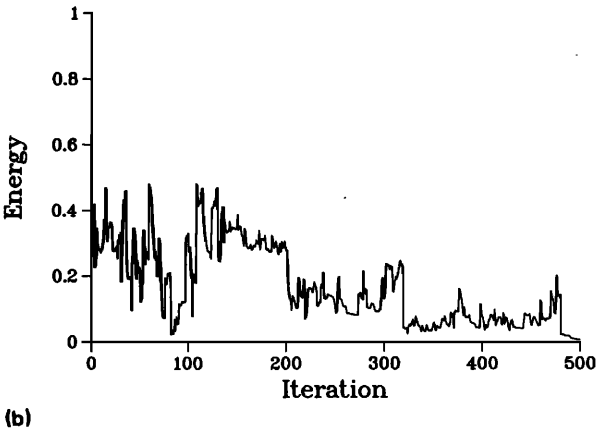

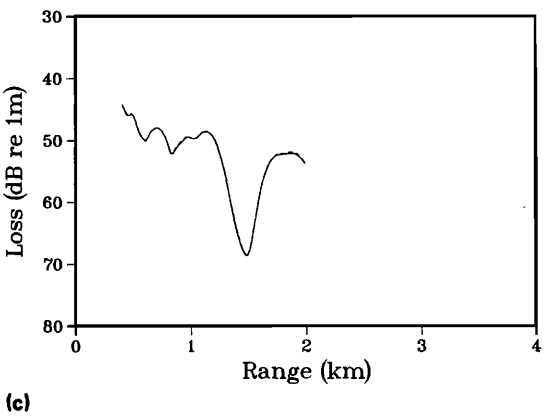

FIG. 7. Results for example B, which involves a range-independent ocean overlying a two-layer sediment. Inversion using a horizontal array that stretches out to $r = 2$ km. (a) Convergence of the parameters to the true values (dashed lines). (b) The energy function. (c) Transmission loss curves for the parameters corresponding to the lowest energy state encountered (solid curve) and for the true parameters (dashed curve).

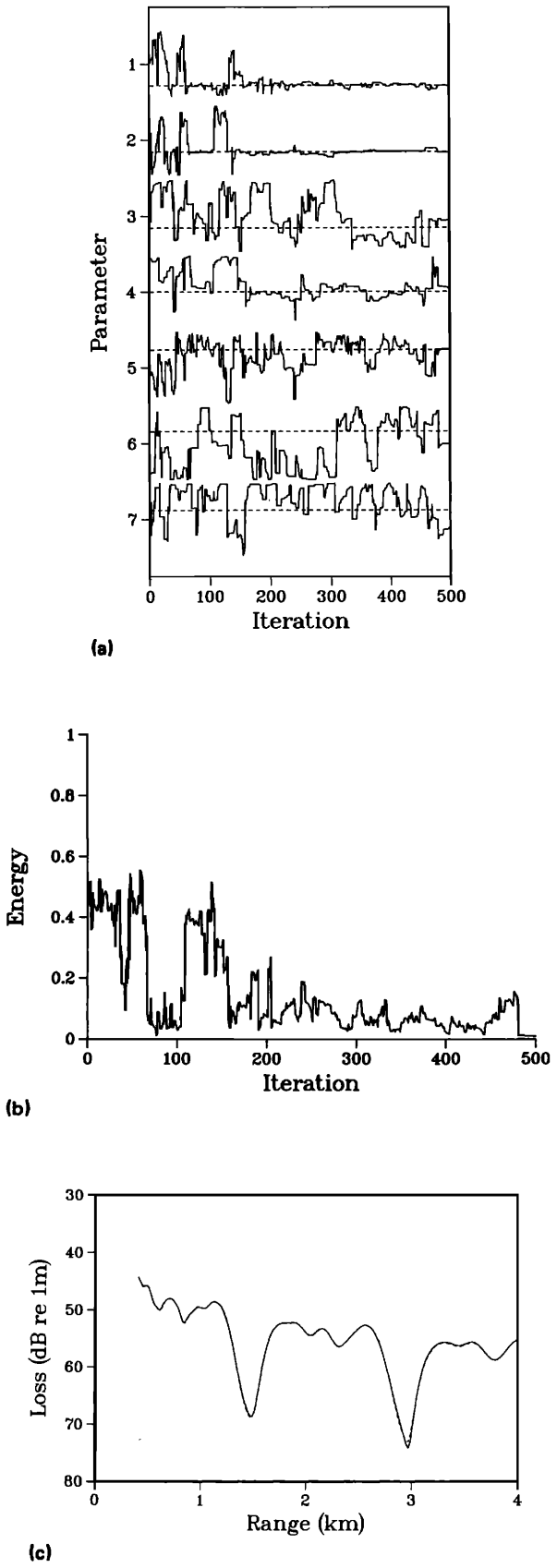

FIG. 8. Results for example B, which involves a range-independent ocean overlying a two-layer sediment. Inversion using a horizontal array that stretches out to $r = 4$ km. (a) Convergence of the parameters to the true values (dashed lines). (b) The energy function. (c) Transmission loss curves for the parameters corresponding to the lowest energy state encountered (solid curve) and for the true parameters (dashed curve).

ing was quenched after 480 iterations. Some of the parameters become stronger attractors (i.e., X_j tends to remain close to Y_j) as the length of the array increases. The additional data obtained by increasing the array length is redundant, however, and the values of $\tilde{X}_j$ appearing in Table II do not improve as array length increases. The 4-km case took 12 min to run on a Cray X-MP/24 computer.

III. APPLICATION TO GULF OF MEXICO DATA

In this section, we apply the PE-based inversion method to data from a gradually range-dependent region of the Gulf of Mexico. Lynch *et al.* took the data and analyzed it with a linear inversion method and a range-independent propagation model.[3] The data set consists of 5-km synthetic aperture arrays at two depths and two frequencies. We decided to consider the higher frequency of 140 Hz because the 50-Hz data appear to contain more noise and less information (the modal interference pattern contains little structure at 50 Hz because the ocean depth is only about 30 m). Prior to the experiment, Matthews *et al.* estimated the sediment parameters of the region using various types of information.[23] Rubano performed an earlier acoustic experiment in the region.[24]

The sound speed was measured at approximately $c_w = 1545$ m/s throughout the water column.[3] In the upper layer of the sediment, the sound speed is similar to the sound speed in the water column and the attenuation is small.[23] Thus the upper layer is effectively an extension of the water column in the acoustical sense. A well-defined boundary divides the upper layer and the lower layer, which has higher values for c, ρ, and β.[23] We experimented with various parametrizations and found that the variable depth of the interface between the upper and lower sediment layers is an important parameter. Without accounting for this range dependence, we were able to match the data only for short ranges. We found evidence that a sound-speed boundary layer exists in the top part of the upper sediment layer. In the boundary layer, the sound speed changes relatively rapidly from the value at the interface to a relatively gradually varying background sound-speed profile.

With the PE-based inversion method, it should be possible to obtain a good estimate of the sediment parameters by working with data from only a fraction of the 5-km interval. In order to compare our results with the results of Ref. 3, however, we chose to work with the entire 5-km interval. We used the data from the receiver at $z = 15.3$ m. Although the second receiver at $z = 28.8$ m adds no further information in principle, these data are useful in practice. After performing inversion using the data from one of the receiver depths, the data at the other receiver depth may be compared with the replica field predicted by the inverted sediment parameters. This is a useful test of the quality of the data.

As illustrated in Fig. 9, sixteen parameters were used to describe the environment. Table III contains parameters and results for this problem. The upper layer lies within $d_1(r) < z < d_2(r)$, where the continuous functions d_1 and d_2 are linear over the segments $0 < r < 2.5$ km and $2.5 < r < 5$ km. At the three endpoints of the segments, d_1 has the values

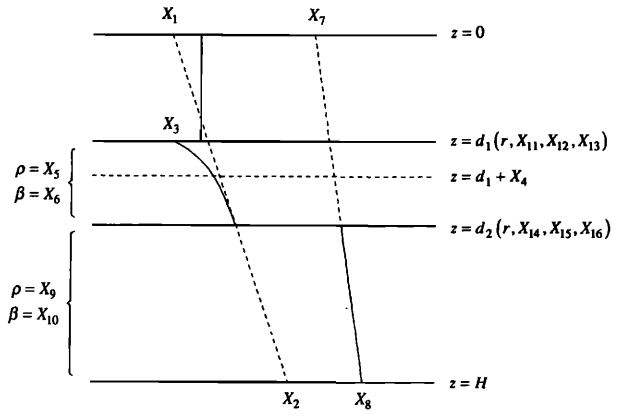

FIG. 9. Parametrization for a problem involving data from the Gulf of Mexico. The sound speed in the water column ($z<d_1$) is known from direct measurement. The sound speed in the upper layer of the sediment ($d_1<z<d_2$) is assumed to have a boundary layer. The sound speed in the lower layer ($z>d_2$) is assumed to be linear. The solid horizontal lines represent the boundaries of the layers. The dashed horizontal line represents the extent of the boundary layer. The solid nonhorizontal curves represent the sound-speed profile. The dashed nonhorizontal lines represent the background profile for the upper layer and the profile for the lower layer.

X_{11}, X_{12}, and X_{13} and d_2 has the values X_{14}, X_{15}, and X_{16}. The following sound-speed profile[25] was used to model the boundary layer:

$$c(r,z)=c_0+(X_3c_w-c_0)\exp\left(-2\frac{z-d_1}{X_4}\right), \quad (6)$$

$$c_0(z)=X_1+(X_2-X_1)z/H, \quad (7)$$

where $H=100$ m is the depth at which the computational grid was truncated. The background sound-speed profile c_0 is referenced to the points $z=0$ and $z=H$ because the depths that would be more natural for this purpose, the locations of the interfaces, are range dependent. Over the boundary layer of thickness X_4, the sound speed rapidly varies from the value X_3c_w at the top of the upper layer to the background sound-speed profile. In the lower layer, the sound speed is modeled by

$$c(z)=X_7+(X_8-X_7)z/H. \quad (8)$$

In the upper layer, ρ and β correspond to X_5 and X_6. In the lower layer, ρ and β correspond to X_9 and X_{10}.

We applied the simulated annealing algorithm to solve this problem using the energy function defined by Eq. (5) and $T_0=10$. We performed 525 iterations and quenched the annealing after 500 iterations. We used the data from $0.2<r<5$ km. For this problem, the run time on a Cray X-MP/24 was about 1.3 h. This time could be reduced significantly by designing a PE code to handle the range-dependent environment more efficiently or by performing the inversion over a shorter range interval. The parameter intervals used for simulated annealing and the parameter values corresponding to the lowest energy state encountered appear in Table III. The results of the inversion appear in Figs. 10 and 11.

The data and replica transmission loss curves are in excellent agreement for both receiver depths. The agreement for the second receiver suggests that the data set is of high quality. Although the minimum energy achieved is only moderately small, a significant fraction of the residual energy appears to be due to noise in the data. The sound-speed profile at $r=0$ is in reasonable agreement with the profile predicted in Ref. 23 and the profile obtained by inversion in Ref. 3. Since the inversion was performed using a single frequency, however, this profile probably lacks some of the finer details in the upper layer (which could be resolved with higher frequencies) and some of the major details of the deeper layer (which could be resolved with lower frequencies).

The value of 0.971 obtained for X_3, which is a strong attractor, is lower than the value of 0.987 stated in Ref. 23. There are several possible explanations for this difference: it might be difficult to measure quantities in a boundary layer (especially if the existence of the boundary layer is not suspected); this quantity might be difficult to resolve with the data and the model we applied in the inversion; the boundary-layer sound-speed profile might not be valid for this environment. The range of values for d_2-d_1, the thickness of the upper layer, is larger than the value stated in Ref. 23. One possible explanation for this difference is that this quantity is range-dependent, and the value of Ref. 23 is for a nearby location. The fact that X_{14}, X_{15}, and X_{16} are strong attractors in the simulated annealing search suggests that the values for $\tilde{X}_{14}$, $\tilde{X}_{15}$, and $\tilde{X}_{16}$ appearing in Table III are close to the true values.

Since X_5, X_9, and X_{10} are relatively weak attractors, it is not significant that the values obtained for these parameters are not identical to the values stated in Ref. 23. Since the upper layer acts like an extension of the water column, X_6 is a strong attractor. Since bathymetry data were provided by Lynch *et al.*, we placed small intervals around X_{11}, X_{12}, and X_{13} and found these parameters to be relatively weak attractors. Since the physics of the boundary layer is not fully understood, we can not speculate on the accuracy of the value obtained for X_4.

TABLE III. The parameters for a problem involving data from a range-dependent region of the Gulf of Mexico and inversion with the PE method.

j	$\tilde{X}_j$	A_j	B_j	Units
1	1547.2	1450	1550	m/s
2	1573.0	1500	1650	m/s
3	0.971	0.97	1.01	
4	19.0	5.0	20.0	m
5	1.66	1.46	1.66	g/cm^3
6	0.034	0.0	0.1	dB/λ
7	1644.6	1600	1700	m/s
8	1687.5	1650	1750	m/s
9	1.76	1.74	1.94	g/cm^3
10	0.103	0.1	0.5	dB/λ
11	30.7	29.8	30.8	m
12	28.6	28.5	29.5	m
13	27.0	26.0	27.0	m
14	54.8	40.0	60.0	m
15	48.6	40.0	60.0	m
16	45.1	40.0	60.0	m

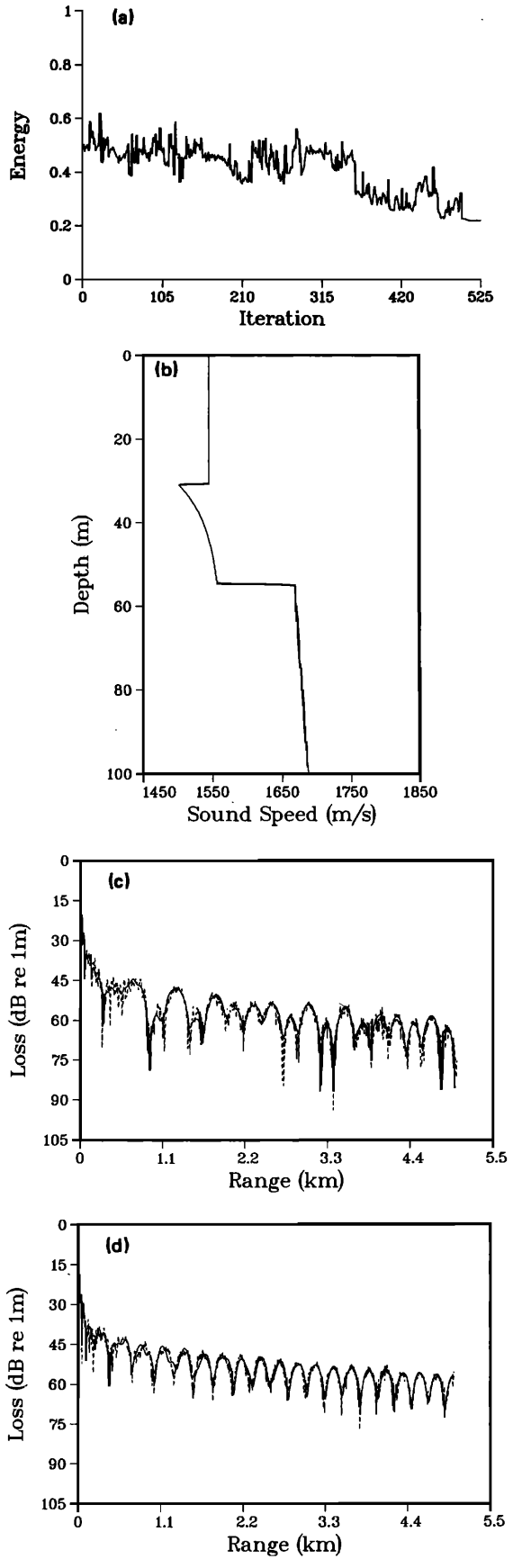

FIG. 10. Results for a problem involving data from the Gulf of Mexico. Inversion using a horizontal array that stretches out to $r = 5$ km. (a) The energy function. (b) The recovered sound-speed profile at $r = 0$. (c) Transmission loss for the receiver used for the inversion. (d) Transmission loss for the second receiver. The transmission loss curves correspond to the lowest energy state (solid curves) and the data (dashed curves).

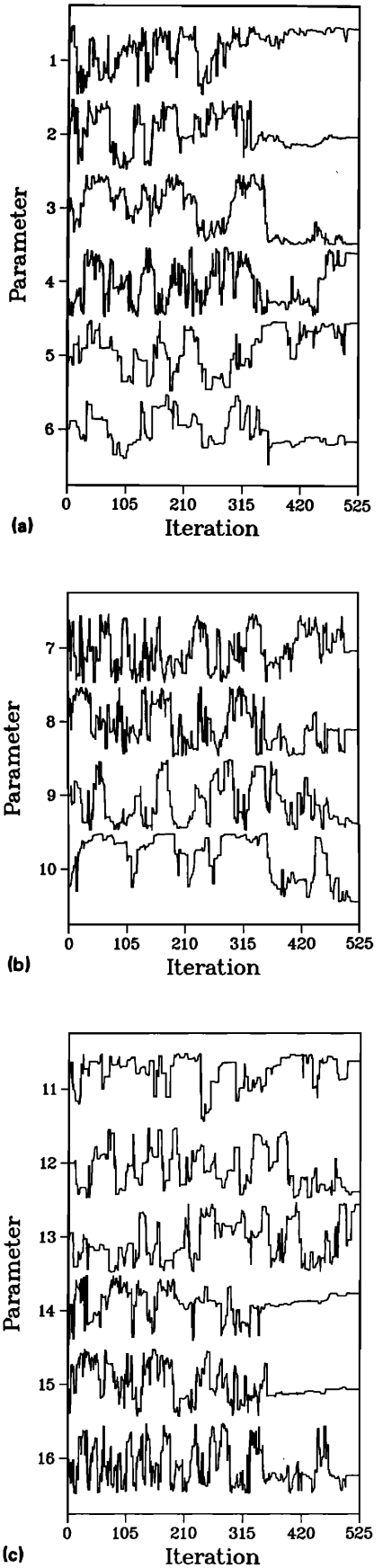

FIG. 11. Results for a problem involving data from the Gulf of Mexico. Inversion using a horizontal array that stretches out to $r = 5$ km. (a) The parameters of the upper layer. (b) The parameters of the lower layer. (c) The interface parameters.

IV. INVERSION IN WAVE-NUMBER SPACE

In this section, we describe an inversion algorithm based on matching the wave-number spectrum, which is applicable to problems that are range independent in the region $r < r_0$. The complex pressure $P(r)$ is measured on a horizontal array of receivers that spans $r < r_0$. It is necessary to measure phases for this approach. The wave-number spectrum $p(h)$ is defined by

$$p(h) = \int_0^\infty r J_0(rh) P(r) dr. \tag{9}$$

Unless the range-independent region is very large, it is not possible to approximate the integral in Eq. (9) by truncating the integration path to $r < r_0$. If the range-independent region extends out to the far-field region that is dominated by normal-mode propagation, however, the integrand may be extrapolated using the far-field normal-mode solution,[21]

$$P(r) \cong r^{-1/2} \sum_{m=1}^{M} A_m \exp(ik_m r). \tag{10}$$

The complex quantities A_m and k_m are estimated by minimizing the following energy function:

$$E = \sqrt{\sum_{j>j_0} \left| P_j - r_j^{-1/2} \sum_{m=1}^{M} A_m \exp(ik_m r_j) \right|^2}, \tag{11}$$

where the receivers in the far-field region correspond to $j > j_0$. This frequency-domain beamforming problem may be solved accurately and efficiently with simulated annealing.[26,27] This high-resolution approach requires less data than other approaches for solving this problem.[28] This advantage is important if the range-independent region is relatively small. If the environment is range dependent for $r > r_0$, the extrapolated field does not correspond to the true field.

Using Eq. (10) and the large-argument approximation for the Bessel function, we obtain the following estimate for the wave-number spectrum:

$$p(h) = \int_0^{r_0} r J_0(rh) P(r) dr + \sqrt{\frac{2}{\pi h}} \sum_{m=1}^{M} A_m \times \int_{r_0}^{\infty} \cos\left(rh - \frac{\pi}{4}\right) \exp(ik_m r) dr, \tag{12}$$

$$p(h) = \int_0^{r_0} r J_0(rh) P(r) dr + \sqrt{\frac{2}{\pi h}} \sum_{m=1}^{M} \frac{A_m \exp(ik_m r_0)}{k_m^2 - h^2} \times \left[ik_m \cos\left(r_0 h - \frac{\pi}{4}\right) + h \sin\left(r_0 h - \frac{\pi}{4}\right) \right]. \tag{13}$$

The vectors $\mathbf{p}$ and $\mathbf{q}$ contain the wave-number spectrum data and replica sampled at the N points h_n, and the energy is defined by

$$E = \sqrt{1 - |\hat{\mathbf{p}}^* \hat{\mathbf{q}}|^2}. \tag{14}$$

Since it is usually necessary to compute the wave-number spectrum for thousands of wave-number samples to accurately construct the complex pressure, it is possible to improve efficiency by working in wave-number space and performing inversion using perhaps a few tens of wave-number samples.

TABLE IV. The parameters for example C, which involves a two-layer sediment (the same environment as example B) and inversion in wave-number space. The values for $\tilde{X}_j$ appear in separate columns for the θ windows of 20 to 40 deg and 30 to 50 deg.

j	Y_j	A_j	B_j	20/40	30/50	Units
1	1530	1500	1650	1514.6	1549.7	m/s
2	1600	1550	1700	1610.9	1582.0	m/s
3	1.2	1.1	1.4	1.40	1.16	g/cm^3
4	0.05	0.0	0.1	0.050	0.069	dB/λ
5	1750	1600	1800	1750.5	1749.9	m/s
6	1.4	1.15	1.5	1.50	1.33	g/cm^3
7	0.35	0.1	0.5	0.249	0.339	dB/λ

Example C involves the ocean environment of example B. As in example B, the 50-Hz source is at $z = 25$ m and the array is at $z = 95$ m. Table IV contains parameters (defined in example B) and results for example C. We take $h_n = k_w \cos\theta_n$, and $N = 20$, where k_w is the wave number in the water column, and consider the cases $\theta_n = (18 + 2n)$ deg and $\theta_n = (28 + 2n)$ deg. We applied the simulated annealing algorithm to solve this problem using the energy function defined by Eq. (14) and $T_0 = 10$. We performed 500 iterations and quenched the annealing after 480 iterations. Results for the two sampling intervals appear in Figs. 12 and 13. For the case in which the steeper angles are sampled, X_3, X_5, and X_7 are stronger attractors. For the other case, X_4 is a stronger attractor.

For both of the cases, X_1 and X_2 are correlated because the solution is slightly ambiguous. The energy function is relatively insensitive to variations in c for which the average value of $c(z)$ in the upper layer is constant. This ambiguity does not appear in the results for example B. Otherwise, the performance of the two approaches is similar for this problem. We constructed replicas for example C using the spectral model of Ref. 15, which solves the depth boundary value problem using finite differences. The run time for this approach is insensitive to the complexity of the depth-dependent environment. The run time of 5 min on a Cray X-MP/24 computer is less than half the run time required to solve the 4-km case with the PE method.

The spectral model of Refs. 19 and 20 solves the boundary value problem with analytic functions. If the number of homogeneous layers (linear variations in c^{-2} are permitted in fluid layers) required to describe the environment is not too large, this approach is much faster than the finite-difference approach. For example, this model, which handles elastic ocean bottoms, required only 20 s of run time on a Cray X-MP/24 computer to solve example C.

We apply the spectral model of Refs. 19 and 20 to example D, which involves a 5-Hz source at $z = 95$ m in a 100-m-deep ocean overlying an elastic bottom. The receiver is at $z = 100$ m and $c = 1500$ m/s in the water column. The elas-

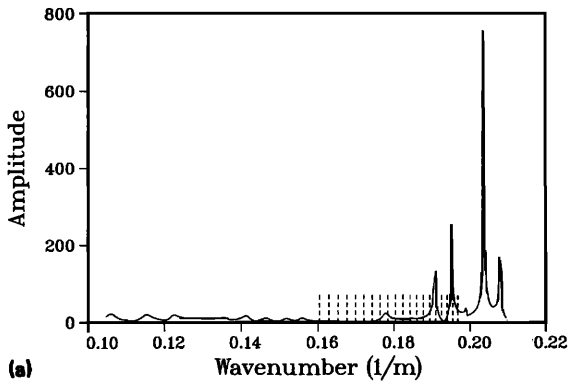

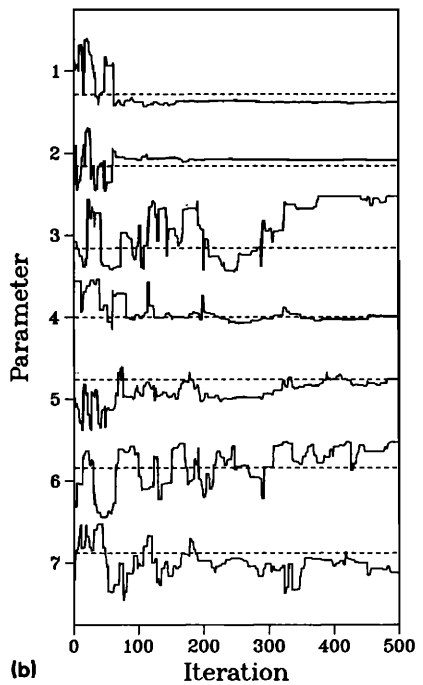

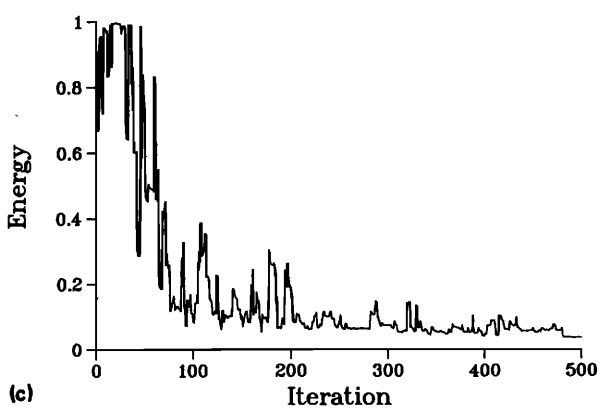

FIG. 12. Results for example C, which involves a range-independent ocean overlying a two-layer sediment (the same environment as example B). Inversion using wave numbers corresponding to $20 < \theta < 40$ deg. (a) The wave-number spectrum (solid curve) and the sampled points (dashed markers). (b) Convergence of the parameters to the true values (dashed lines). (c) The energy function.

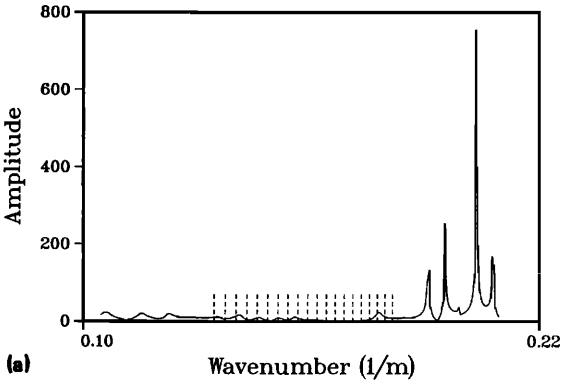

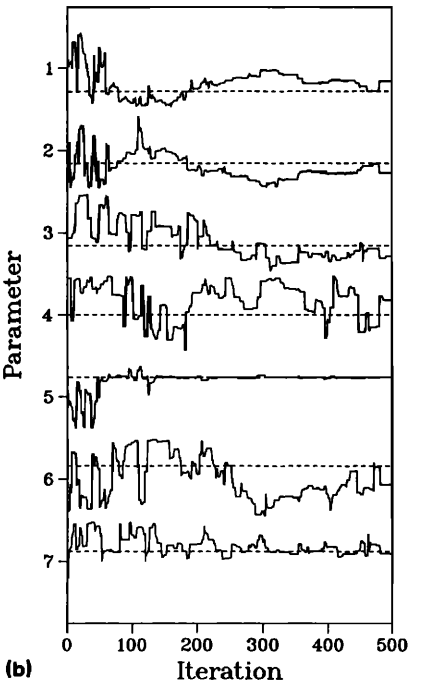

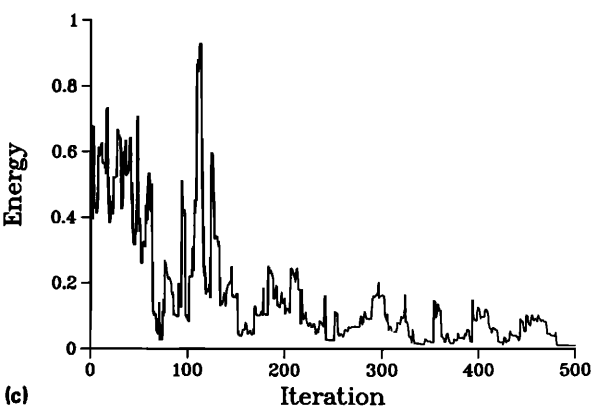

FIG. 13. Results for example C, which involves a range-independent ocean overlying a two-layer sediment (the same environment as example B). Inversion using wave numbers corresponding to $30 < \theta < 50$ deg. (a) The wave-number spectrum (solid curve) and the sampled points (dashed markers). (b) Convergence of the parameters to the true values (dashed lines). (c) The energy function.

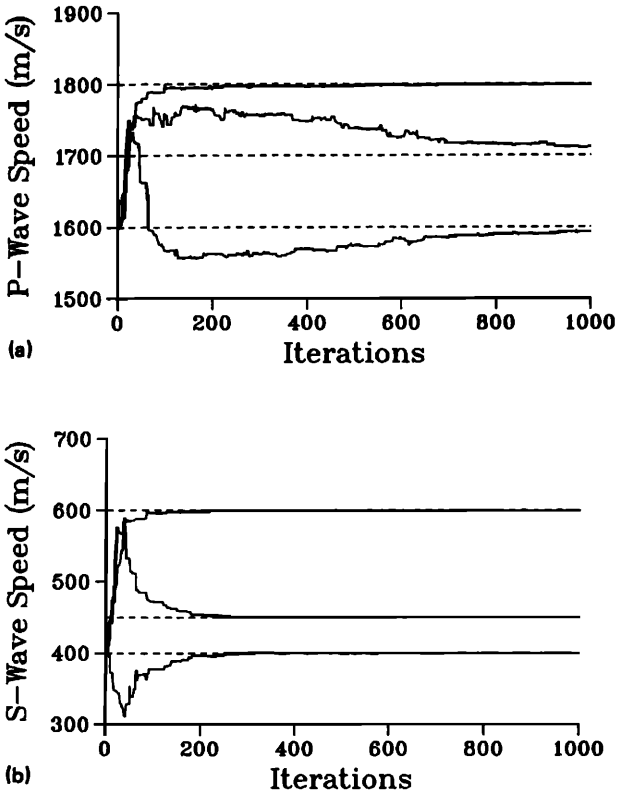

FIG. 14. Results for example D, which involves a three-layer elastic bottom. (a) Convergence of the compressional speeds. (b) Convergence of the shear speeds.

tic bottom consists of two 10-m-thick layers overlying a homogeneous half-space. In the respective layers, the compressional speeds are 1600, 1700, and 1800 m/s, the shear speeds are 400, 450, and 600 m/s, the densities are 1.8, 1.9, and 2 g/cm^3, the compressional attenuations are 0.2, 0.15, and 0.1 dB/λ, and the shear attenuations are 0.5, 0.4, and 0.2 dB/λ.

We assumed that the densities and attenuations are known *a priori* and used 16 equally spaced wave-number samples corresponding to phase speeds between 300 and 3000 m/s. The results for 1000 iterations appear in Fig. 14. The shear speeds are strong attractors because the phase speed of the interface wave is sensitive to shear speed variations. The compressional speed in the lower layer is also a strong attractor, and the compressional speed in the two upper layers is resolved fairly well. The run time for example D was 10 s on a Cray X-MP/24 computer.

V. CONCLUSION

Nonlinear inversion methods have been developed and tested using simulated and real data. The inversion method based on the PE method is applicable to realistic range-dependent problems. Although a large number of PE runs are required, the total run time is within practical limitations because the runs are out to short ranges. The PE-based inversion method was applied to data from the Gulf of Mexico. The replica fields corresponding to the lowest energy encountered are in excellent agreement with the data. The recovered sediment parameters are in reasonable agreement with the parameters predicted by Matthews *et al.* and inverted for by Lynch *et al.* The results of the inversion suggest that the depth of the interface between the upper two layers of sediment decreases with range and that a sound-speed boundary layer exists in the upper part of the upper layer. It would be worthwhile to collect additional data from this region, preferably for various frequencies, and perform further inversion studies. A method for performing nonlinear inversion in wave-number space, which is applicable to range-independent segments, was developed and tested on simulated data. This method is efficient because the number of wave-number samples required for inversion is a small fraction of the number of wave-number samples required to construct solutions of the wave equation.

ACKNOWLEDGMENTS

The authors thank J. Lynch, S. Rajan, and G. Frisk for providing their data and for helpful discussions.

APPENDIX A: SIMULATED ANNEALING

In this Appendix, we describe the simulated annealing algorithm that we have developed for nonlinear inversion for ocean-bottom properties. Additional background information can be found in Ref. 27. The steps in the algorithm include randomly perturbing the parameters, evaluating the change ΔE in the energy function, deciding whether to accept the perturbation, and lowering the temperature T. The jth parameter X_j is required to remain within the interval (A_j,B_j). At the nth iteration, the parameters are perturbed one at a time with the perturbed value of X_j being

$$X_j' = X_j + \Delta X_j \sigma_{n,j}^3, \tag{A1}$$

where ΔX_j is the maximum possible perturbation and a random number generator is used to select the numbers $\sigma_{n,j}$ uniformly from the interval $(-1,1)$. The fast simulated annealing cooling schedule[29] is $T = T_0/n$, where the initial temperature T_0 is an important control parameter. For fast simulated annealing to be effective, it is necessary to choose ΔX_j to be relatively large. We have found that $\Delta X_j = \frac{1}{2}(B_j - A_j)$ is an effective choice. If the perturbed parameter is outside the interval, it is reflected back into the interval as follows:

$$X_j' \rightarrow \begin{cases} 2B_j - X_j', & \text{if } X_j' > B_j, \\ 2A_j - X_j', & \text{if } X_j' < A_j. \end{cases} \tag{A2}$$

This reflection procedure prevents the endpoints of the interval from being attractors.

Each parameter is designated either unique or nonunique. The energy function is assumed to achieve a single local minimum as a unique parameter is varied throughout its interval while the other parameters are held fixed. Perturbations that lower the energy are always accepted for both parameter types. Perturbations of unique parameters are always rejected if the energy is raised. For a nonunique parameter, a perturbation that produces an energy increase is accepted if

$$\tau_{n,j} < \exp(-\Delta E/T). \tag{A3}$$

This is the usual acceptance condition for simulated annealing algorithms. A random number generator is used to select the numbers $\tau_{n,j}$ uniformly from the interval (0,1). Increases in energy are more likely to be accepted at higher temperatures. The convergence of simulated annealing is determined by the distribution of the perturbations and by the cooling schedule. The inverse-linear cooling schedule is effective if the distribution of perturbations includes many small perturbations (to sample local gradients) and some large perturbations (to leap out of local minima). The cubic distribution given by Eq. (A1) has these properties.

APPENDIX B: RADIATION BOUNDARY CONDITIONS

In this Appendix, we derive RBCs that are useful for the inversion problem. The following factors should be considered when designing RBCs for ocean acoustics problems: the values of c in the water column and at the bottom of the computational grid usually differ significantly; RBCs break down for grazing incidence (usually the most important case in ocean acoustics) and perform the best for normal incidence (often the most important case for the inversion problem); the accuracy of a particular RBC depends on the parabolic approximation used in the interior of the computational grid.

The spreading factor $r^{-1/2}$ is removed from the acoustic pressure, which satisfies the farfield Helmholtz equation,

$$\left(\frac{\partial^2}{\partial r^2} + \frac{\partial^2}{\partial z^2} + k^2\right) P = 0, \tag{B1}$$

for $kr \gg 1$. An outgoing signal satisfies the following factorization of Eq. (B1):

$$\frac{\partial P}{\partial r} = ik_0\sqrt{1 + X^2 + Y^2}\,P, \tag{B2}$$

$$X = k_0^{-1}\frac{\partial}{\partial z}, \tag{B3}$$

$$Y^2 = k_0^{-2}(k^2 - k_0^2), \tag{B4}$$

where k_0 is a representative wave number.

Applying a rational-linear approximation[15,30,31] for the square-root operator in Eq. (B2), we obtain the higher-order PE:

$$\frac{\partial P}{\partial r} = ik_0\left(1 + \sum_{j=1}^{n} \frac{a_{j,n}(X^2 + Y^2)}{1 + b_{j,n}(X^2 + Y^2)}\right) P, \tag{B5}$$

where $a_{j,n}$ and $b_{j,n}$ are constants and n is increased to improve accuracy. The higher-order PE is useful in the interior of the computational grid. Since the higher-order PE involves two depth derivatives, however, it is not useful as an RBC. The following approximation may be used as an RBC:

$$\frac{\partial P}{\partial r} = ik_0\left(1 + \frac{\alpha X}{1 + \beta X} + \gamma\right) P. \tag{B6}$$

Although other forms of rational-linear functions may be useful as RBCs, stability problems can arise.[32] We assume that the acoustic parameters are independent of depth near the bottom of the grid so that Y^2 is a constant. We determine the coefficients α, β, and γ by requiring that the following approximation satisfies accuracy constraints:

$$f(X) \equiv \sum_{j=1}^{n} \frac{a_{j,n}(X^2 + Y^2)}{1 + b_{j,n}(X^2 + Y^2)} \cong \frac{\alpha X}{1 + \beta X} + \gamma \equiv g(X). \tag{B7}$$

In ocean acoustics, the limit $X \to 0$ (i.e., small propagation angles) is usually the most important case. The approximation given by Eq. (B6) breaks down in this limit[22] (i.e., total reflection occurs). The approximation does not break down for nongrazing angles, however, and is most effective for normal incidence. In particular, this RBC significantly reduces reflections from the bottom boundary at short ranges. By requiring that $f(X) - g(X) = f'(X) - g'(X) = f''(X) - g''(X) = 0$ at $X = X_0 = i\sin\theta$, where θ is the optimized propagation angle ($\theta = 90$ deg corresponds to normal incidence), we obtain

$$\beta = \frac{-f''(X_0)}{X_0 f''(X_0) + 2f'(X_0)}, \tag{B8}$$

$$\alpha = (1 + \beta X_0)^2 f''(X_0), \tag{B9}$$

$$\gamma = f(X_0) - \frac{\alpha X_0}{1 + \beta X_0}. \tag{B10}$$

Other types of constraints, such as the ones used in Ref. 22, are useful for different ranges of incidence angles.

For a plane wave incident on the bottom boundary, the reflection coefficient R is given by[22]

$$R = -\frac{f(X) - g(X)}{f(X) - g(-X)}. \tag{B11}$$

The reflection amplitude $|R|$ appears in Fig. B1 for the case $\theta = 70$ deg and $n = 1$. The complex Padé coefficients of Ref. 15 were used for $a_{j,n}$ and $b_{j,n}$. Also appearing in Fig. B1 is the reflection amplitude that corresponds to using the Helmholtz equation in the interior and using the RBC designed for the PE. Since the PE is accurate to about 40 deg for $n = 1$, the two reflection amplitudes agree for $\theta < 40$ deg. For the PE, $|R| \ll 1$ is very small for $\theta > 60$ deg because the RBC is designed for the PE. For the Helmholtz equation, $|R|$ is relatively large near normal incidence.

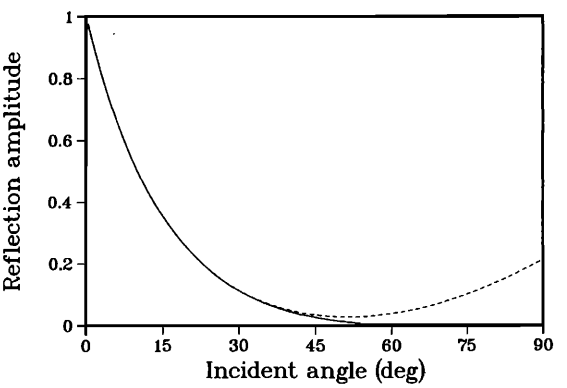

FIG. B1. Reflection amplitudes for a radiation boundary condition designed for the PE. The solid curve corresponds to using the PE in the interior of the domain. The dashed curve corresponds to using the Helmholtz equation in the interior of the domain.

APPENDIX C: THE ENERGY FUNCTION

This Appendix contains a derivation of Eq. (4) from Eq. (3). We define $F = |\mathbf{P} - \lambda \mathbf{Q}|^2$ and express $\lambda = A \exp(i\theta)$ in terms of the real quantities A and θ to obtain

$$E^2 = |\mathbf{P}|^{-2} \min_{A,\theta} F(A,\theta), \tag{C1}$$

$$F = |\mathbf{P}|^2 - A \exp(i\theta)\mathbf{P}^*\mathbf{Q} - A\exp(-i\theta)\mathbf{Q}^*\mathbf{P} + A^2|\mathbf{Q}|^2. \tag{C2}$$

The conditions for minimizing F are

$$0 = \frac{\partial F}{\partial \theta} = -iA \exp(i\theta)\mathbf{P}^*\mathbf{Q} + iA \exp(-i\theta)\mathbf{Q}^*\mathbf{P}, \tag{C3}$$

$$0 = \frac{\partial F}{\partial A} = -\exp(i\theta)\mathbf{P}^*\mathbf{Q} - \exp(-i\theta)\mathbf{Q}^*\mathbf{P} + 2A|\mathbf{Q}|^2. \tag{C4}$$

The value $\lambda = |\mathbf{Q}|^{-2}\mathbf{Q}^*\mathbf{P}$ follows from these equations. Substituting into Eq. (C2), we obtain

$$E^2 = 1 - |\hat{\mathbf{P}}^*\hat{\mathbf{Q}}|^2. \tag{C5}$$

[1] D. C. Stickler, "Inverse scattering in a stratified medium," J. Acoust. Soc. Am. **74**, 994–1005 (1983).

[2] S. D. Rajan, J. F. Lynch, and G. V. Frisk, "Perturbative inversion methods for obtaining bottom parameters in shallow water," J. Acoust. Soc. Am. **82**, 998–1017 (1987).

[3] J. F. Lynch, S. D. Rajan, and G. V. Frisk, "A comparison of broadband and narrow-band modal inversions for bottom properties at a site near Corpus Christi, Texas," J. Acoust. Soc. Am. **89**, 648–665 (1991).

[4] N. R. Chapman and K. Rohr, "Measurement of the elastic properties of the ocean bottom by inversion of reflection amplitude data," in *Shear Waves in Marine Sediments*, edited by J. M. Hovem, M. D. Richardson, and R. D. Stoll (Kluwer, Dordrecht, 1991), pp. 537–544.

[5] A. Caiti, T. Akal, and R. D. Stoll, "Determination of shear velocity profiles by inversion of interface wave data," in Ref. 4, pp. 557–566.

[6] H. P. Bucker, "Use of calculated sound fields and matched-field detection to locate sound sources in shallow water," J. Acoust. Soc. Am. **59**, 368–373 (1976).

[7] A. B. Baggeroer, W. A. Kuperman, and H. Schmidt, "Matched field processing: Source localization in correlated noise as an optimum parameter estimation problem," J. Acoust. Soc. Am. **83**, 571–587 (1988).

[8] M. D. Collins and W. A. Kuperman, "Focalization: Environmental focusing and source localization," J. Acoust. Soc. Am. **90**, 1410–1422 (1991).

[9] A. Tolstoy, O. Diachok, and L. N. Frazer, "Acoustic tomography via matched field processing," J. Acoust. Soc. Am. **89**, 1119–1127 (1991).

[10] N. Metropolis, A. W. Rosenbluth, M. N. Rosenbluth, A. H. Teller, and E. Teller, "Equations of state calculations by fast computing machines," J. Chem. Phys. **21**, 1087–1091 (1953).

[11] S. Kirkpatrick, C. D. Gellatt, and M. P. Vecchi, *Optimization by Simulated Annealing* (IBM Thomas J. Watson Research Center, Yorktown Heights, NY, 1982).

[12] D. H. Rothman, "Nonlinear inversion, statistical mechanics, and residual statics estimation," Geophysics **50**, 2784–2796 (1985).

[13] A. Basu and L. N. Frazer, "Rapid determination of critical temperature in simulated annealing inversion," Science **249**, 1409–1412 (1990).

[14] F. D. Tappert, "The parabolic approximation method," in *Wave Propagation and Underwater Acoustics*, edited by J. B. Keller and J. S. Papadakis, Lecture Notes in Physics, Vol. 70 (Springer-Verlag, New York, 1977).

[15] M. D. Collins, "Higher-order Padé approximations for accurate and stable elastic parabolic equations with application to interface wave propagation," J. Acoust. Soc. Am. **89**, 1050–1057 (1991).

[16] M. D. Collins and E. K. Westwood, "A higher-order energy-conserving parabolic equation for range-dependent ocean depth, sound speed, and density," J. Acoust. Soc. Am. **89**, 1068–1075 (1991).

[17] G. V. Frisk and J. F. Lynch, "Shallow water waveguide characterization using the Hankel transform," J. Acoust. Soc. Am. **76**, 205–216 (1984).

[18] W. A. Kuperman, M. F. Werby, K. E. Gilbert, and G. J. Tango, "Beam forming on bottom-interacting tow-ship noise," IEEE J. Ocean. Eng. **10**, 290–298 (1985).

[19] H. Schmidt and F. B. Jensen, "A full wave solution for propagation in multilayered viscoelastic media with application to Gaussian beam reflection at fluid-solid interfaces," J. Acoust. Soc. Am. **77**, 813–825 (1985).

[20] H. Schmidt, "SAFARI user's guide," SACLANTCEN SR-113, SACLANT Undersea Research Centre, La Spezia, Italy (1988).

[21] R. B. Evans, "A coupled mode solution for acoustic propagation in a waveguide with stepwise depth variations of a penetrable bottom," J. Acoust. Soc. Am. **74**, 188–195 (1983).

[22] R. W. Clayton and B. Engquist, "Absorbing boundary conditions for wave-equation migration," Geophysics **45**, 895–904 (1980).

[23] J. E. Matthews, P. J. Bucca, and W. H. Geddes, "Preliminary environmental assessment of the Project GEMINI site—Corpus Christi, Texas," NORDA TR-120, Naval Ocean Research and Development Activity, Stennis Space Center, Mississippi (1985).

[24] L. A. Rubano, "Acoustic propagation in shallow water over a low-velocity bottom," J. Acoust. Soc. Am. **67**, 1608–1613 (1980).

[25] M. D. Collins, H. B. Ali, M. J. Authement, A. Nagl, H. Überall, J. F. Miller, and J. I. Arvelo, "Low-frequency sound interaction with a sloping, refracting ocean bottom," IEEE J. Ocean. Eng. **13**, 235–244 (1988).

[26] K. C. Sharman, "Maximum likelihood parameter estimation by simulated annealing," in *Proceedings of the IEEE Conference on Acoustics, Speech, and Signal Processing* (IEEE, New York, 1988), pp. 2741–2744.

[27] W. A. Kuperman, M. D. Collins, J. S. Perkins, and N. R. Davis, "Optimal time-domain beamforming with simulated annealing including application of *a priori* information," J. Acoust. Soc. Am. **88**, 1802–1810 (1990).

[28] M. D. Collins, W. A. Kuperman, J. S. Perkins, N. C. Makris, and N. R. Davis, "Optimal time-domain beamforming with simulated annealing including noise cancellation," in *Proceedings of the Institute of Acoustics*, edited by R. Lawrence (Rayross, Liverpool, 1991), pp. 259–265.

[29] H. Szu and R. Hartley, "Fast simulated annealing," Phys. Lett. **122**, 157–162 (1987).

[30] J. F. Claerbout, *Fundamentals of Geophysical Data Processing* (McGraw-Hill, New York, 1976), pp. 206–207.

[31] A. Bamberger, B. Engquist, L. Halpern, and P. Joly, "Higher order paraxial wave equation approximations in heterogeneous media," SIAM J. Appl. Math. **48**, 129–154 (1988).

[32] L. H. Howell and L. N. Trefethen, "Ill-posedness of absorbing boundary conditions for migration," Geophysics **53**, 593–603 (1988).